SCIENTIFIC REPORTS

OPEN

Rotational dynamics and dynamical transition of water inside hydrophobic pores of carbon nanotubes

Haruka Kyakuno[1,2], Kazuyuki Matsuda[2], Yusuke Nakai[1], Ryota Ichimura[1], Takeshi Saito[3], Yasumitsu Miyata[1,4], Kenji Hata[5] & Yutaka Maniwa[1]

Water in a nanoconfined geometry has attracted great interest from the viewpoint of not only basic science but also nanofluidic applications. Here, the rotational dynamics of water inside single-walled carbon nanotubes (SWCNTs) with mean diameters larger than ca. 1.4 nm were investigated systematically using ^{2}H nuclear magnetic resonance spectroscopy with high-purity SWCNTs and molecular dynamics calculations. The results were compared with those for hydrophilic pores. It was found that faster water dynamics could be achieved by increasing the hydrophobicity of the pore walls and decreasing the pore diameters. These results suggest a strategy that paves the way for emerging high-performance filtration/separation devices. Upon cooling below 220 K, it was found that water undergoes a transition from fast to slow dynamics states. These results strongly suggest that the observed transition is linked to a liquid-liquid crossover or transition proposed in a two-liquid states scenario for bulk water.

Water in a nanoconfined geometry exhibits unusual dynamical properties that do not appear in the bulk. Studies of this type of water are useful to design high-performance filtration/separation devices[1–3] and to reveal the function of hydrophobic biological channels[4–6]. They are also of significant interest with respect to the basic science of water. Water in the bulk has many anomalous properties, such as a density maximum at 277 K. Some scenarios, including the hypothesis of a critical point between two-liquid states present in a deeply super-cooled regime, have been proposed to understand these anomalies[7–9]. However, experimental studies are hampered by a region (150–235 K at ambient pressure) where bulk water inevitably crystallizes. Alternatively, because nanoconfinement suppresses the crystallization of water, many theoretical and experimental studies have been performed in confinement geometries[10–21], such as water in pores of silica, zeolites, and nanocarbons, and water on protein surfaces. However, a collective view on these properties has not yet been achieved[16–18]. In particular, systematic studies on the effect of pore dimensions, temperature, and the hydrophobicity of material surfaces on water dynamics are rather limited.

In the present study, water inside single-walled carbon nanotubes (SWCNTs) was employed to systematically reveal water dynamics inside "hydrophobic" nanocavities[22]. SWCNTs provide cylindrical pores whose diameter D can be systematically controlled from less than 1 nm to a few nanometers. Water inside SWCNTs exhibits several phases upon cooling from room temperature (RT)[23–28]. For thin SWCNTs ($D <$ ca. 1.45 nm), liquid water adsorbed at RT is transformed upon cooling into tubule ices with a one-dimensional periodicity, and are referred to as ice-nanotubes (ice-NTs). For thick SWCNTs ($D >$ ca. 1.45 nm), on the other hand, water exhibits a wet-dry transition or a hydrophilic–hydrophobic transition at around 220–240 K[22,28], and the water is partially ejected from the inside of the SWCNTs. However, a substantial quantity of water can be trapped inside the SWCNTs even below the wet-dry transition temperature. Here, this water inside SWCNTs was investigated by nuclear magnetic

[1]Department of Physics, Graduate School of Science and Engineering, Tokyo Metropolitan University, Hachioji, 192-0397, Japan. [2]Institute of Physics, Faculty of Engineering, Kanagawa University, Yokohama, 221-8686, Japan. [3]Nanomaterials Research Institute, National Institute of Advanced Industrial Science and Technology, Tsukuba, 305-8565, Japan. [4]JST, CREST, Kawaguchi, 332-0012, Japan. [5]CNT-application Research Center, National Institute of Advanced Industrial Science and Technology, Tsukuba, 305-8565, Japan. Correspondence and requests for materials should be addressed to H.K. (email: h-kyakuno@kanagawa-u.ac.jp) or Y.M. (email: maniwa@phys.se.tmu.ac.jp)
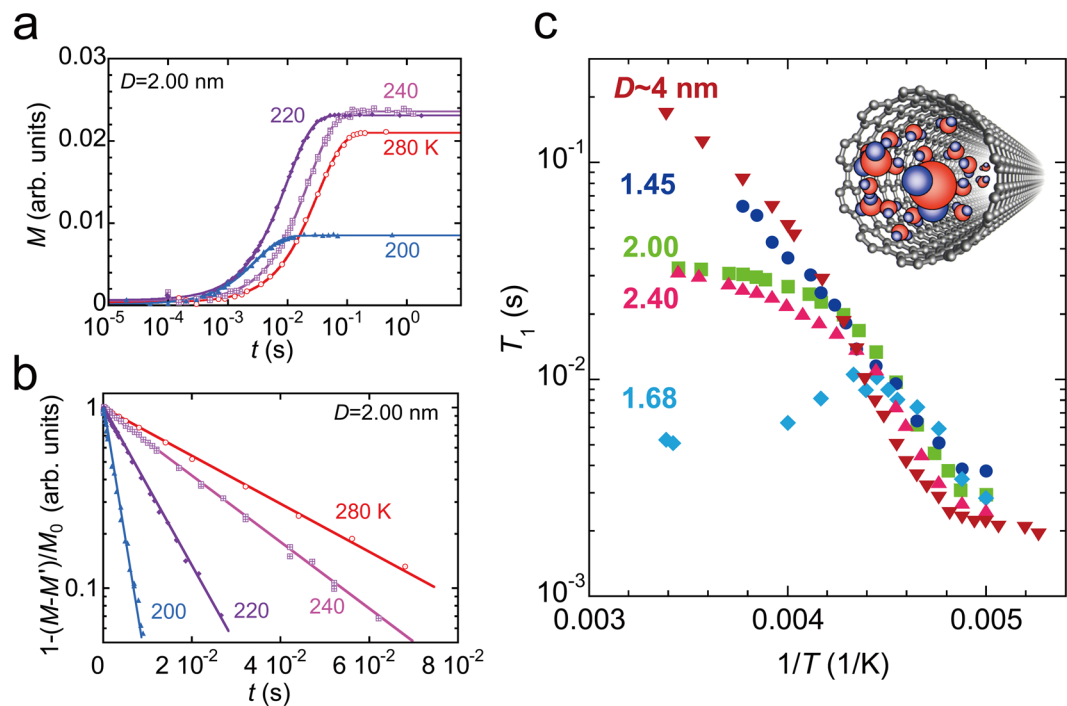
Figure 1. ^{2}H-NMR results for water-SWCNTs. (**a** and **b**) Relaxation curves measured for the SWCNT sample with a mean diameter of $D = 2.00$ nm. The solid lines are fitted with equation (1). (**c**) Spin-lattice relaxation time T_1, obtained for the SWCNT samples with $D = 1.45$, 1.68, 2.00, 2.40, and 4 nm as a function of $1/T$. The inset shows a schematic illustration of a SWCNT with water molecules. D is the mean SWCNT diameter in the sample.

resonance (NMR) spectroscopy[29,30] to clarify the water dynamics. It is known that NMR spectroscopy enables the study of large-amplitude molecular motions on the time scale of 10^{-5}–10^{-11} s. In water-SWCNTs, the narrowed NMR spectra of water that can be observed even below the bulk freezing temperature have been assigned to liquid or mobile water inside SWCNTs[28,31–37].

In the present study, we used high-purity SWCNT samples[38–40] because magnetic impurities present in SWCNT samples, such as residual metal catalysts used in the synthesis of SWCNTs[41], often prevents their intrinsic properties from being observed by NMR spectroscopy. ^{2}H-NMR measurements were performed on heavy water inside SWCNT samples. The results are discussed to evaluate the role of hydrophobicity of the pore walls and pore diameters in the water dynamics and transition, in combination with molecular dynamics (MD) calculations, differential scanning calorimetry (DSC) measurements, X-ray diffraction (XRD) analysis, and data previously reported for hydrophilic pores of MCM-41.

Results and Discussion

NMR spin-lattice relaxation time, T_1. The ^{2}H-T_1 of heavy water inside SWCNTs was measured as a function of temperature T and SWCNT diameter D to probe large-amplitude molecular rotation. Figure 1a shows examples of the raw data acquired to determine T_1 values. NMR signal intensity, $M(t)$, which is proportional to the nuclear magnetization along the applied static magnetic field, was measured as a function of time t, after a saturation comb pulse, and was fitted with equation (1) (in *Methods*) to obtain T_1, M', β, and M_0. Figure 1b shows $\log\{1-[M(t)-M']/M_0\}$ as a function of t. All the measurements presented here give $\beta \approx 0.95$–0.99, as approximately reproduced by the straight lines for $\beta = 1$ in Fig. 1b. This implies that T_1 is homogeneous and independent of water sites, or averaged over different water sites inside a SWCNT by the moving or hopping of water molecules within the T_1 process, ca. 10^{-3}–10^{-1} s. The small deviation from $\beta = 1$ may be due to the distribution of SWCNT diameters in the sample because the water dynamics are expected to be somewhat dependent on the SWCNT diameter.

Figure 1c summarizes the T-dependences obtained for the different diameter SWCNT samples. At low temperatures, all the samples show a similar T-dependence, which can be described by the Bloembergen-Purcell-Pound (BPP) relaxation mechanism[29,30,42] with the T-dependent rotational correlation time of water molecules τ_{rot}, in equation (2) (in *Methods*). On the other hand, the T-dependence in the higher-T regions is unusual; the T_1 values do not change systematically with the SWCNT diameter, and these may be correlated to the content of magnetic impurities (see Supplementary Fig. S1). For instance, the T_1 of the magnetically impure samples ($D = 1.68$, 2.00, and 2.40 nm) is substantially shorter than that of the high-purity samples ($D = 1.45$ and 4.0 nm). This suggests that the magnetic impurities dominate the T_1 mechanisms of impure samples in the higher-T regions. Note that the observed T_1 may be given by $(1/T_1) = (1/T_1)_{imp} + (1/T_1)_{BPP}$, where $(1/T_1)_{imp}$ and $(1/T_1)_{BPP}$ are contributions from magnetic impurities and BPP mechanism, respectively. With
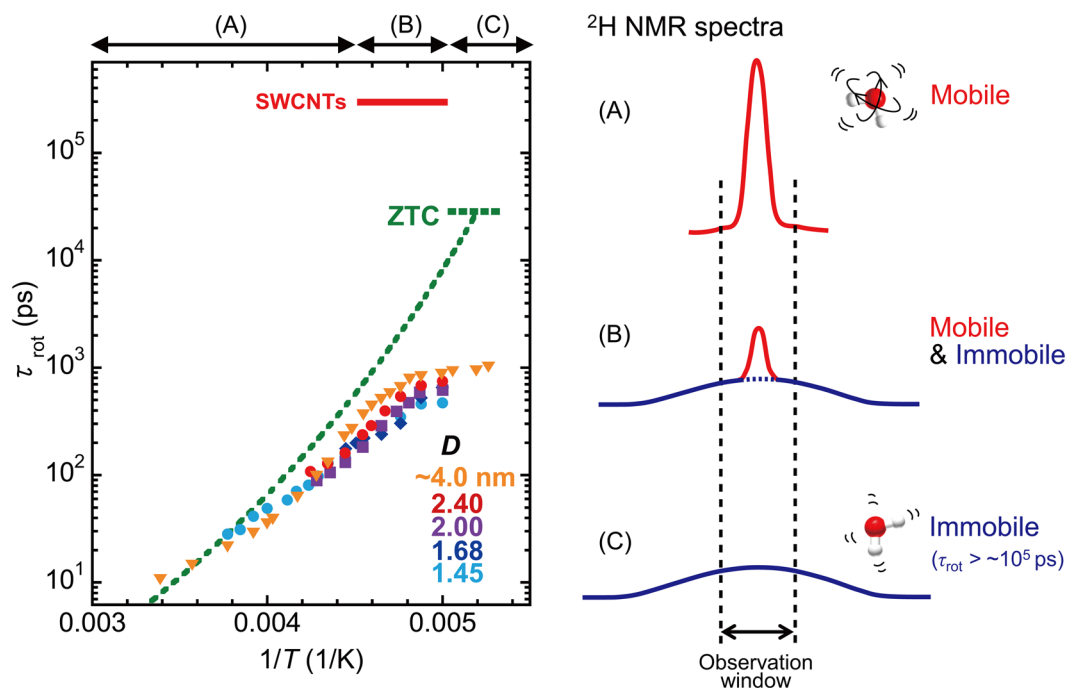
Figure 2. Rotational correlation time (τ_{rot}) of water molecules inside SWCNTs obtained by ^{2}H-NMR. The SWCNT mean diameters are $D = 1.45$, 1.68, 2.00, 2.40, and ~4.0 nm. The dotted line shows the rotational correlation time of water confined inside the three-dimensional pore geometry of zeolite-templated carbon (ZTC) for comparison[45]. The horizontal lines represent the estimated rotational correlation times from the line-broadenings in the SWCNTs and ZTC. The observation window used in ZTC was 2 kHz. Right: Schematic illustrations of the NMR spectra in three temperature regions (**A**), (**B**), and (**C**) shown in the left figure. Only the narrow spectra shown in red are detected in the present measurement setup. Region (**A**): All water molecules have $\tau_{rot} < \sim 10^3$ ps, and give the narrow NMR spectra. Region (**B**): there are mobile water with $\tau_{rot} < \sim 10^3$ ps and immobile water with $\tau_{rot} > \sim 10^5$ ps. Although the present T_1-measurement setup can detect $\tau_{rot} < \sim 10^5$ ps, τ_{rot} of $\sim 10^3 - \sim 10^5$ ps was not observed in the present samples. It is strongly suggested that the τ_{rot} discontinuously changes in the T-region (**B**).

lowering temperature, $(1/T_1)_{BPP}$ steeply increases as expected from equation (2) through the strong T-dependence of τ_{rot}. Thus $(1/T_1)_{BPP}$ dominates the observed $1/T_1$ at low temperatures. Therefore, discussions in the following sections focus on the low-T data.

The rotational correlation time, τ_{rot}, which is estimated from the observed T_1 using equation (2) (in *Methods*) for the BPP relaxation mechanism, is summarized in Fig. 2. The value ($\tau_{rot} = 10$–20 ps) extrapolated to 273–300 K is slightly longer than that of bulk water (2–6 ps)[43], but substantially shorter than a value (ca. 100 ns) reported in a previous NMR study on water inside a SWCNT sample[44]. This discrepancy in the NMR results for water-SWCNTs is probably due to different conditions used for equation (2) to estimate τ_{rot}. Although equation (2) has two possible solutions for τ_{rot} for each T_1 value, the present measurements of T-dependence enabled us to unambiguously select the correct value for τ_{rot}. The discrepancy may also be due to the difference in sample quality used in the experiments.

Upon cooling, τ_{rot} increases but it is still shorter than $\sim 10^3$ ps down to 200 K, where the NMR signal almost disappears due to broadening of the NMR spectra. The T-dependence of τ_{rot} is described by the Arrhenius T-dependence, $\tau_{rot} \propto \exp(B/k_B T)$ with an activation energy B, although weak deviations from the Arrhenius law are clearly observed in Fig. 2. It is also found that τ_{rot} depends on the SWCNT diameter D. With larger D, the T-dependence of τ_{rot} becomes steeper. These features are qualitatively reproduced by MD calculations, which are presented later.

The value $\tau_{rot} \approx 3 \times 10^5$ ps is also obtained from the broadening condition of NMR spectra (see *Methods*), as indicated by the horizontal lines in Fig. 2. As shown in Supplementary Fig. S2 and reported in ref.[28], the NMR signal intensity diminishes at low temperatures and almost disappears at ca. 200 K in all the samples studied. This implies that the NMR spectra were broadened over the instrumental observation windows of ~20 kHz by slowing of the water rotational motion to $\tau_{rot} > \sim 3 \times 10^5$ ps. Therefore, this result indicates that almost all the water transforms into a slow dynamics state at 200 K.

The above estimation for τ_{rot} from the NMR linewidth and T_1 indicates that there are two water states with different mobilities at low temperatures: one is mobile water, which gives the narrowed spectra with $\tau_{rot} \approx 10^3$ ps, and the other is an immobile (or less mobile) water, which gives unobservable spectra, with $\tau_{rot} > \sim 3 \times 10^5$ ps. It is particularly important to realize that there is no evidence for the existence of water molecules with $\tau_{rot} \approx 10^3$–10^5 ps over the whole temperature range examined. Therefore, we conclude that the mobile water at high T
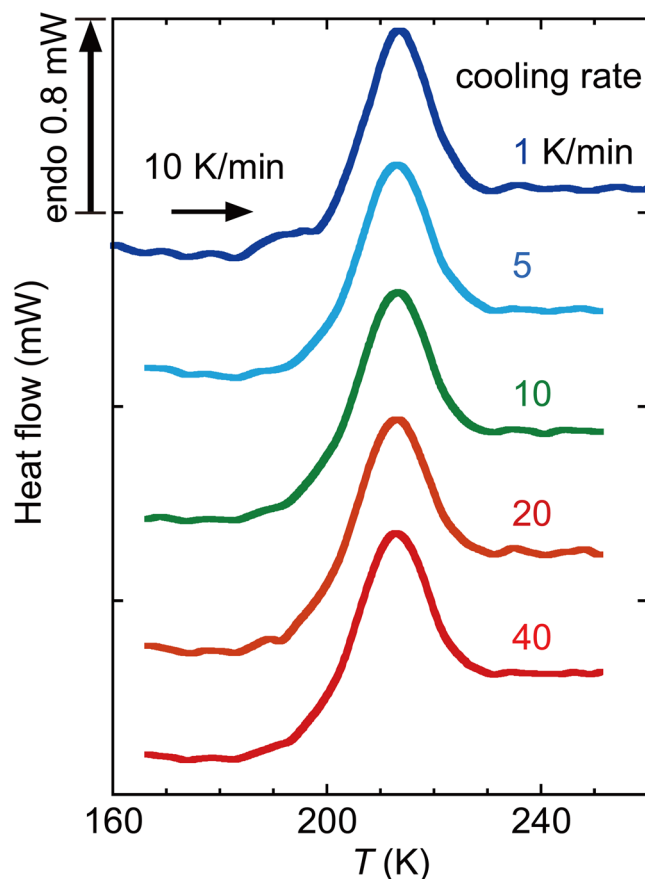
Figure 3. The DSC curves of 2.18 nm SWCNTs as a function of cooling rate. The DSC cell was filled with excess water to inhibit the wet-dry transition.

transforms into immobile water upon cooling with a sudden change in τ_{rot}. This is quite different from the case where water freezes gradually, as in a glass transition. In that case, τ_{rot} increases gradually upon cooling, as reported in confined water in zeolite-templated carbon (ZTC) with three-dimensional pores[45], shown by the dashed line in Fig. 2. The observed features in water-SWCNTs indicate a discontinuous transition between mobile (liquid) water and immobile (solid or less mobile liquid) water.

It is worth noting that the observed two water states are essentially stable within the NMR-T_1 time scale which is larger than 10^{-3} s. Besides, the two types of water can be assumed to form finite-size domains, respectively, so that the observed XRD patterns are reproducible as a superposition of corresponding two distinct XRD patterns (see Supplementary Fig. S5). These features, along with the discontinuous change in water dynamics, are consistent with those of a first-order phase transition. The broad coexisting T-region (200–220 K) of mobile and immobile water molecules, observed in the present experiments, could be explained by any inhomogeneities present in the samples, such as distributions of SWCNT diameters and water occupations inside SWCNTs[28] which can cause a distribution of transition temperature. However, because of lack of convincing evidence for origin of the broad T-region, further examinations should be required to rule out other possibilities such as a continuous transition[46], in which the content ratio of two types of water changes continuously with temperature inside each SWCNT.

DSC measurements. DSC measurements were performed to characterize the transition observed in the NMR measurements. Figure 3 shows the results for a water-SWCNT sample. After cooling to 130 K at different cooling rates, DSC curves were recorded with heating at 10 K/min, and an endothermic peak was clearly observed around 200–225 K, which suggests a phase transition. Under the present sample conditions, the wet-dry transition was inhibited because the DSC cell was filled with excess water, such that the openings of the SWCNTs were stoppled with bulk ice[22]. Thus, the peak was assigned to the transition of water inside the SWCNTs and not to the wet-dry transition. In addition, no evidence was found for a glass transition because the endothermic peak was not affected by the cooling time.

MD calculations of τ_{rot}. Classical MD calculations were performed to examine the microscopic picture of the molecular dynamics. Figure 4a shows τ_{rot} calculated for the SPC/E water[47] confined in SWCNTs with several diameters, along with that of ZTC[45]. We found the following features from the calculated τ_{rot} as functions of D and T. For SWCNTs with $D \leq 1.41$ nm, the water undergoes liquid-solid transitions upon cooling and forms ordered tubular ices (ice NTs) at low temperatures and thus τ_{rot} increases steeply below the transition temperature (see
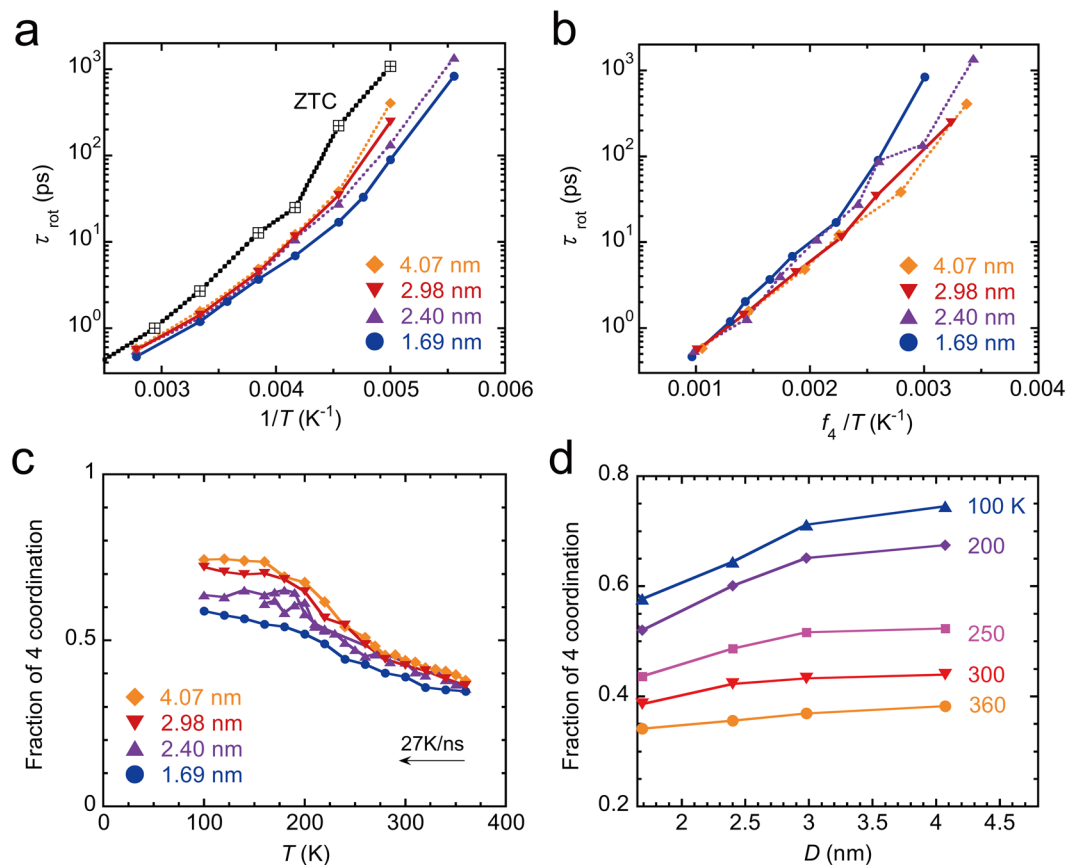
Figure 4. Results of MD calculations for water inside SWCNTs with diameters of 1.69, 2.40, 2.98, and 4.07 nm. (**a**) Calculated rotational correlation time ($\tau_{\rm rot}$) as a function of T. The result for water inside ZTC is also shown for comparison. (**b**) T-dependence of $\tau_{\rm rot}$ as a function of f_4 / T. (**c**) and (**d**) Calculated fraction of four coordination water molecules, f_4. Water inside SWCNTs with $D \leq 1.41$ nm is transformed into tubular ices (ice NTs) at low-T (see Supplementary Fig. S3).

Supplementary Fig. S3a). In larger diameter SWCNTs ($D > 1.6$ nm), $\tau_{\rm rot}$ shows non-Arrhenius T-dependence and is better described by a Vogel-Fulcher-Tammann (VFT) form, $\tau_{\rm rot} = \tau_0 \, \exp[B/(T-T_0)]$. As D increases, $\tau_{\rm rot}$ as a function of $1/T$ becomes steeper. In addition, a comparison between ZTC and SWCNTs suggests that the pore topology plays an important role on the molecular dynamics. The $\tau_{\rm rot}$ for ZTC with a three-dimensional pore exhibits a stronger T-dependence than those of SWCNTs with one-dimensional pores. All these features qualitatively explain the experimental observations as shown in Fig. 2.

Figure 4c,d show the fraction of four-coordination water molecules f_4, where the four-coordination water is defined as a molecule having four neighboring molecules with the O-O distance shorter than 0.33 nm. f_4 can be used as an indicator of the fraction of water molecules that contribute to hydrogen-bonding. f_4 increases for all the SWCNTs with a decrease in T, which indicates that a hydrogen-bonding network develops at lower temperatures. For SWCNTs with $D > 1.6$ nm, f_4 increases with D (Fig. 4d), which implies that the larger diameter SWCNT has a weaker geometrical restriction for the formation of a hydrogen-bonding network.

The observed non-Arrhenius behavior of $\tau_{\rm rot}$ may be partially related to the development of such a hydrogen-bonding network with the temperature. As D increases, $\tau_{\rm rot}$ increases along with f_4. Figure 4b shows $\tau_{\rm rot}$ tentatively plotted as a function of f_4 / T. The T-dependence at least at high-T can be roughly described by $\tau_{\rm rot} = \tau_0 \exp[E_0 f_4 /(k_B T)]$, where E_0 is a constant. This implies that the activation energy, $E_0 f_4$, for the reorientation increases with lowering of the temperature as a result of an increase in f_4 or the development of hydrogen bonds. The value for E_0/k_B is in the range of 2500–2900 K and is almost equal to the binding energy for a typical hydrogen bond, 2400 K. The deviation from linearity at low-T may be related to the transition observed in the present experiments.

Role of hydrophobicity. Here, we discuss the effect of pore hydrophobicity on the water dynamics. The large diameter SWCNTs are hydrophobic, particularly at low temperatures[22]; therefore, a comparison of the present results with those for hydrophilic MCM-41 with a similar one-dimensional pore geometry is instructive. The correlation times are compared in Fig. 5a.

It is found from Fig. 5a that the dynamics of the confined water are quite different between CNT systems, including both SWCNT and double-walled carbon nanotubes (DWCNT)[48], and the MCM-41 systems[49,50]. The
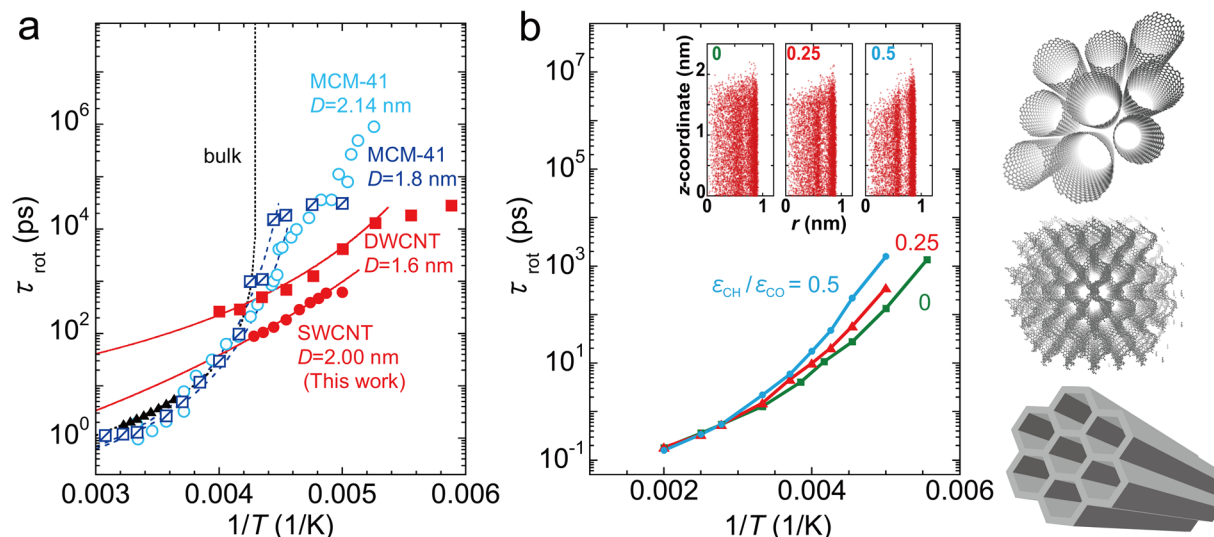
Figure 5. Temperature dependence of correlation times for confined water. (**a**) Comparison of correlation times for water inside SWCNTs, DWCNTs[48], MCM-41[49,50], and bulk water[43]. Data represented by circles (MCM-41, $D = 2.14$ nm; SWCNT, $D = 2.00$ nm) and triangles (bulk water) were determined from ^{2}H-NMR measurements, while those represented by squares (MCM-41, $D = 1.8$ nm; DWCNT, $D = 1.6$ nm) were from quasielastic neutron scattering (QENS) measurements. The dashed and solid lines are fitted with $\tau_{rot} = \tau_0 \exp[B/(T - T_0)]$ at high-T regions. (**b**) τ_{rot} of water inside a 2.00 nm SWCNT as a function of pore hydrophilicity, obtained from MD calculations. The interaction parameters, ε_{CH}, between a carbon atom in a SWCNT and a hydrogen atom in water were taken as $\varepsilon_{CH}/\varepsilon_{CO} = 0$, 0.25, and 0.50. Insets show the menisci of the confined water molecules at 285 K. r is the distance from the symmetry axis or the tube axis of the SWCNT, and z is the coordinate along the tube axis. Right: schematic illustrations of a SWCNT bundle, ZTC, and MCM-41 from top to bottom, respectively.

water inside CNTs exhibits weaker T-dependences than in MCM-41, and has a shorter correlation time at low-T, i.e., water is highly mobile at low-T in hydrophobic CNTs. The behavior of water in MCM-41 is closer to that of bulk super-cooled water with a singularity around 230 K (see dotted line in Fig. 5a). The effect of hydrophobicity is presumably explained by the different interaction strength between water and the pore walls. In the hydrophobic pores of CNTs, water cannot be bonded to the CNT walls because the dominant interaction between water and carbon atoms in the wall is the van der Waals interaction, which is much weaker than water-water interactions, whereas water molecules are easily bonded or anchored to the silanol groups in the wall of MCM-41. As a result, water inside hydrophobic pores can be more mobile, particularly at low temperatures.

To further support the above discussion, τ_{rot} was calculated for SWCNTs with different pore hydrophobicities (Fig. 5b). Here, the hydrophobicity was artificially varied through the use of different interaction parameters between carbon atoms in the SWCNTs and hydrogen atoms in water. This interaction induces water molecules to anchor to the SWCNT wall. As the carbon-hydrogen interaction increases, the meniscus changes toward that observed with hydrophilic pores (see the insets of Fig. 5b), and the T-dependence of τ_{rot} becomes steeper. This is consistent with the present observations and previous reports[49–51]. Similar tendencies have been reported in previous MD calculations[52,53].

Transition temperature, T_C, as a function of SWCNT diameter, D. In the range of T where the NMR and DSC measurements confirmed the transition, XRD results have suggested a structural transition (see Supplementary Figs S4 and S5, and ref.[22]). An analysis of water diffuse scattering (WDS) patterns arising from water inside SWCNTs provided a consistent result with the NMR measurements, where the WDS patterns can be decomposed into two components corresponding to the higher- and lower-T structures (see Supplementary Fig. S5). This coincidence indicates that the dynamical transition inferred from the present NMR study is closely related to the structural change at T_C observed by XRD.

As shown in Supplementary Fig. S4 and a previous study[22], WDS patterns change significantly at T_C. Above T_C, the WDS profiles are broad and similar to those for bulk liquid water, whereas they become narrow below T_C. Accordingly, the WDS peak position gradually decreases upon cooling above T_C toward the lower-Q side, and then it shows little change with temperature below T_C. Although these XRD results suggest a structural transition from a liquid state to a solid state, the detailed low-T structures have not been identified at present. Multiwalled helical ice structures, which have been suggested to exist inside SWCNTs by computer simulations[26], are clearly ruled out as the low-T structure by a comparison of the observed and calculated XRD patterns (see Supplementary Fig. S6). Hexagonal ice (ice Ih) structures confined inside SWCNTs may be another candidate for the low-T structure. However, energetically stable ice Ih structures inside SWCNTs, which are compatible with the observed XRD patterns, have not been obtained at present. The observed patterns are instead rather similar to those reported for MCM-41[54], suggesting that a disordered structure is a candidate for the low-T phase. In
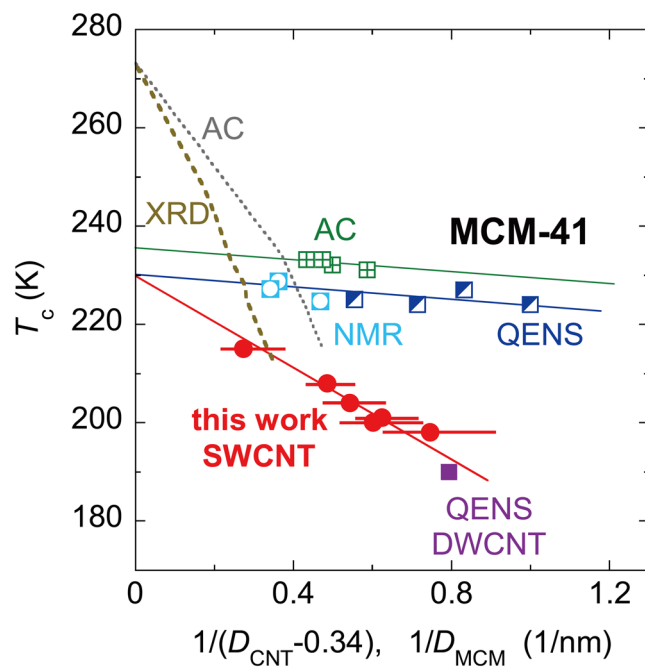
Figure 6. Transition temperature T_C, as a function of pore diameter D', along with distinctive transition temperatures reported previously for water confined in MCM-41. The diameter of the SWCNT pore was defined by $D' = (D-t)$ where $t \approx 0.3 - 0.4$ nm, the thickness of the SWCNT wall. AC: melting temperatures of ice Ih (dotted gray line) and heat-capacity maximum temperatures (green squares with crosses) obtained by adiabatic calorimetry for MCM-41[55]; XRD: melting temperatures of ice Ih obtained from XRD patterns of MCM-41[56]; NMR: anomalous temperatures obtained from NMR relaxation times in MCM-41[49]; QENS: anomalous temperatures obtained from quasielastic neutron scattering measurements[48,50]. The closed red circles were obtained from XRD patterns in ref.[22] and Supplementary Fig. S4 in the present paper.

combination with the NMR results, the water inside SWCNTs presumably exhibits a transition between a mobile liquid state and a less-mobile disordered (liquid or solid) state at T_C.

Next, we discuss the effect of the pore diameter D' on the transition. In SWCNTs, D' is given by $D' = D-t$ with $t \approx 0.34$ nm as the thickness of the SWCNT wall (see *Methods*). Figure 6 plots the T_C as a function of $1/D'$, along with several distinctive transitions or anomalous temperatures reported for water adsorbed inside MCM-41[49,50,55,56] and DWCNTs[48]. The T_C is nearly proportional to $1/D'$, as shown by the straight lines in Fig. 6, similar to the depression of the melting temperature of ice Ih (see thick and thin dashed lines in Fig. 6)[55,56]. When the pore diameter is extrapolated to that of the bulk ($1/D' \to 0$), the T_C for the CNT system, as well as the anomalous temperatures for the MCM-41 system, is ca. 230 K. Interestingly, this is almost equal to a hypothetical singularity temperature of $T_s \approx 228$ K for bulk water[7-9], rather than the melting temperature ($T_m = 273$ K) of ice Ih. This strongly suggests that the nanoconfinement depresses the bulk hypothetical singularity temperature to T_C. The melting (freezing) temperature of ice Ih, if present, may be depressed below T_C in the diameter range of the present SWCNT samples.

By comparing the results for the hydrophobic CNTs and hydrophilic MCM-41 systems, it was found that the depression of T_s by nanoconfinement is much stronger in the CNT system than in the MCM-41 system. In addition, it is worth noting that the discontinuous transition was found at T_c in the present SWCNTs while continuous changes, which may be ascribed to a liquid-liquid crossover (or the Widom line), have been reported in the MCM-41 system[50]. Therefore, it is strongly suggested that the hydrophobicity of pore walls plays an important role in the transition behaviors of confined water, as well as the rotational dynamics. This would be caused through differences in the surface energy between the pore wall and water.

All the above discussions strongly support a scenario that there are two liquid states in water[7-9]. When the temperature passes through the T_s upon cooling, the bulk super-cooled liquid water is transformed into another liquid state (referred to as low density liquid). Upon further cooling, this liquid is presumed to freeze into an amorphous ice (referred to as low density amorphous ice). The present study strongly suggests that the transition between these two liquid states is directly revealed in the nanoconfined geometry.

Conclusions

Confined water inside hydrophobic SWCNTs was studied using ²H-NMR, DSC, XRD measurements, and MD calculations in the temperature range of 300–150 K for SWCNT diameters in the range of 1.45–4.0 nm. Using high-purity SWCNTs, intrinsic information on water dynamics was successfully obtained. It was demonstrated that fast molecular rotation continues until ca. 220 K, and the T-dependence is much weaker than that in the

hydrophilic pores of MCM-41, three-dimensional pores of ZTC, and bulk water. The observed rotational dynamics were well reproduced by MD calculations. Upon cooling below 220 K, water inside the SWCNTs undergoes a transition at T_c, which is dependent on D. The lower-T state is presumably a disordered solid (or liquid) with a rotational correlation time larger than 10^{-7} s. At the limit to the bulk water ($1/D \rightarrow 0$), the T_c is extrapolated to ca. 230 K, the singularity temperature of super-cooled bulk water, which suggests that the nanoconfinement by hydrophobic pores reduces the bulk singularity temperature and leads to a discontinuous dynamical transition. This observation is favorable for the liquid-liquid transition scenario of bulk water[7–9]. The present study established that the hydrophobicity of pore walls and the pore dimensionality have a significant effect on the molecular dynamics of confined water. The results provide information that is helpful not only for the design of high performance nanofluidic devices but also for further studies into the unsolved properties of bulk water.

Methods

Characterization of SWCNT samples.   Experiments were performed on SWCNT samples with mean diameters $D = 1.45 \pm 0.07$, 1.68 ± 0.25, 2.00 ± 0.29, 2.40 ± 0.26 nm[22], and 4 nm. The 4 nm SWCNT sample had a diameter distribution of 3–5 nm[38]. The samples with $D = 1.68$, 2.00, and 2.40 nm were synthesized using the enhanced direct-injection pyrolytic synthesis (eDIPS) method without further purification[39,40]. A previous study involving resonance Raman scattering measurements indicated that SWCNT samples synthesized by the eDIPS method contained relatively few amorphous carbon impurities and few structural defects. The 1.45 nm SWCNT sample (ArcSo grade) was purchased from Meijyo Nanocarbon Ltd., and it was highly purified by a previously reported method[41]. The 4 nm SWCNT sample was synthesized by the super growth (SG) method[38]. Powder XRD patterns for these samples were reported in a previous paper[22] and that for the 4 nm SWCNT sample is given in Supplementary Fig. S4. Magnetic susceptibility measurements were conducted using a superconducting quantum interference device (SQUID) magnetometer (MPMS, Quantum Design) to detect magnetic impurities present in the samples, and the results for the 1.45 and 4 nm samples and a typical eDIPS sample are shown in Supplementary Fig. S1. Compared to the 4 nm SG and purified 1.45 nm samples, the eDIPS samples had larger contents of magnetic impurities.

The raw SWCNTs had few openings (i.e., structural defects) for the introduction of water into the pores; therefore, they were heat-treated in air to open their walls[28]. We presume that these openings are stable at least below RT. The SWCNT samples were sealed in a quartz tube saturated with water vapor after vacuum-pumping down to ca. 1 Pa, except for DSC measurements. The details of this procedure have been reported in previous papers[22,28,33]. The amount of water adsorbed inside the opened SWCNTs with $D = 1.4$–2.4 nm was estimated to be 20–57 wt%, with respect to the dry SWCNTs (see Figs S2–S4 in the Supplementary Material of ref.[22]). The SWCNT diameter D is defined by the centers of carbon atoms in a SWCNT, which implies that the effective pore diameter is given by $D - t$ where $t \approx 0.34$ nm, the thickness of the SWCNT wall.

NMR measurements.   A pulsed Fourier transform NMR technique was used to obtain NMR signals from heavy water in the T-range of 150–300 K. The external magnetic field was 4.0 T, which corresponds to the NMR frequency of $\omega/2\pi = 26.22$ MHz, with a field inhomogeneity of 2–4 ppm over the sample volume. ^{2}H-NMR spectra for water-SWCNTs with $D = 1.4$–2.4 nm have been reported previously[28]. The spectra of the 4 nm SWCNT sample are presented in Supplementary Fig. S2.

In the present study, spin-lattice relaxation times T_1 for deuterons (^{2}H) were used. T_1 relaxation is caused by fluctuating fields at the nuclear sites that are generated by water dynamics[29,30], and the observed time scale easily extends shorter than 10^{-11} s. The T_1 was measured using a saturation recovery method. The recovered nuclear magnetization measured at a time t after the saturation pulses is fitted by a stretched exponential function:

$$M(t) = M_0\{1 - \exp[-(t/T_1)^\beta]\} + M', \tag{1}$$

where M' is an instrumental offset. Here, the NMR intensity or M_0 is inversely proportional to the absolute temperature T and the number of nuclei of interest because the magnitude of nuclear magnetization is well approximated by the Curie law.

To obtain information on molecular dynamics, the Bloembergen-Purcell-Pound (BPP) relaxation mechanism[42] was assumed. Here, the spin-lattice relaxation time is dominated by the quadrupole interaction of ^{2}H nuclei modulated by the molecular reorientations in heavy water because the quadrupole interaction is much larger than other interactions, such as the intra- and inter-molecular dipole-dipole interactions and chemical shielding interactions. Assuming the BPP mechanism, the observed T_1 is given by:

$$\frac{1}{T_1} = \frac{3}{40}\left(\frac{e^2qQ}{\hbar}\right)^2\left(1 + \frac{\eta^2}{3}\right)\left[\frac{\tau_{\text{rot}}}{1 + (\omega\tau_{\text{rot}})^2} + \frac{4\tau_{\text{rot}}}{1 + 4(\omega\tau_{\text{rot}})^2}\right], \tag{2}$$

where the quadrupole coupling constant of $e^2qQ/h = 195$ kHz and its asymmetric parameter of $\eta = 0.1$ are used for heavy water molecules. τ_{rot} is the rotational correlation time of water molecules. The translational diffusion has only a small contribution to the relaxation because the quadrupole coupling interaction is approximately determined by the intramolecular nature of water. However, if magnetic impurities are present in the sample, they can contribute significantly to the relaxation.

The motion of water molecules is also obtained from the phenomena of motional narrowing of the NMR spectrum. When the motion of water molecules is sufficiently slow or static, the NMR spectrum of water in polycrystalline or glassy samples is broadened by nuclear dipole-dipole interactions, electrical quadrupole interactions (for heavy water), and interactions with magnetic impurities when present in the samples. This is because these

interactions generate a magnetic field distribution to which nuclear species of interest are subjected. However, once fast and large amplitude molecular motions start, the NMR spectrum is narrowed because the inhomogeneous field distribution is time-averaged away. This is known as motional narrowing of the NMR spectra. In the case of ^{2}H-NMR measurements with heavy water, this occurs when the time scale of molecular rotational motion typically becomes shorter than 10^{-6} s.

Furthermore, if the instrumental window ΔW to observe the NMR signal is smaller than the width of the NMR spectrum, the observed signal intensity becomes weaker depending on the ΔW. This occurs at $(\tau_{rot} 2\pi \Delta f)\Delta f \sim \Delta W$ where Δf is the width of the static limit, using the extreme narrowing condition. Setting $\Delta f \sim 100$ kHz and $\Delta W \sim 20$ kHz in the present measurements, we obtained $\tau_{rot} \sim 3 \times 10^{-7}$ s $= 3 \times 10^5$ ps. The NMR signal of bulk water, which may exist outside SWCNTs, disappears below 273 K (or 250 K under super-cooling) because $\Delta f \gg \Delta W$ and $\tau_{rot} \gg 3 \times 10^5$ ps. In the present study, thus, it is assumed that the low temperature NMR signal is dominated by liquid-like water confined inside the SWCNTs as reported previously[28,32,36]. Note that the NMR intensity or M_0 in equation (1) is inversely proportional to the absolute temperature T because the nuclear magnetization is well approximated by the Curie law. In a similar way, the NMR signal of water inside the thin SWCNTs (1.4 nm SWCNT sample) disappears at low temperatures due to spectral broadening because the water is transformed into ice-NTs or filled ice-NTs[32].

DSC measurements. DSC measurements were conducted using a calorimeter (DSC 60 Shimadzu Ltd.) in the range of 130–300 K as a function of water content. A typical amount of SWCNT samples was ca. 4 mg, which was sealed inside an aluminum cell with ultrapure water (H_2O). The measurements were conducted under a dry air atmosphere of 0.1 MPa.

MD simulations. The detailed microscopic structure and dynamics of water inside SWCNTs was studied by classical MD simulations using SIGRESS ME 2.3 (Fujitsu Ltd.) for the SPC/E water model[47]. Finite length SWCNTs with diameters of 4.068, 2.983, 2.400, 1.694, 1.411, 1.317, and 1.153 nm, and lengths in the range of 7.166–25.10 nm were investigated. Chiralities of these SWCNTs are (30, 30), (22, 22), (22, 13), (18, 6), (15, 5), (13, 6), and (9, 8), respectively. Calculations were performed in NVT ensembles. The carbon atoms making up the SWCNTs were fixed in the simulation cells and no periodic boundary condition was applied. The potential between the SPC/E water and carbon atoms in SWCNTs was described by the 12–6 Lennard-Jones (LJ) potential: $U_{CO}(r) = 4\varepsilon_{CO}[(\sigma_{CO}/r)^{12} - (\sigma_{CO}/r)^6]$ with parameters of $\varepsilon_{CO}/k_B = 46.88$ K and $\sigma_{CO} = 0.3285$ nm, where k_B is the Boltzmann constant. Here, r is the distance between a carbon atom in a SWCNT and an oxygen atom in water.

The system temperature was gradually decreased from 360 K, where water molecules were highly mobile, down to 100 K with a typical rate of 25–50 K/ns. From the MD results, snapshot structures at each temperature were extracted and they were equilibrated at the temperature for more than 2 ns to calculate rotational correlation functions for the SPC/E water. However, because the correlation time becomes longer with a decrease in the temperature, the water system could not be equilibrated at low temperatures, ca. below 200 K.

The rotational correlation functions $C_\ell(t) = \langle P_\ell[\cos \theta(t)]P_\ell[\cos \theta(0)]\rangle$, where $P_\ell[\cos \theta(t)]$ denotes a Legendre polynomial of rank ℓ, were calculated from the MD results. Here, $C_2(t)$ can be obtained from NMR and light scattering[57], while $C_1(t)$ is obtained from dielectric spectroscopy. Therefore, $C_2(t)$ was compared with the NMR results:

$$C_2(t) = \frac{1}{2}\langle 3\cos^2 \theta(t) - 1\rangle = \frac{1}{2}\langle 3\{\vec{u}_i(t) \cdot \vec{u}_i(0)\}^2 - 1\rangle, \tag{3}$$

where $\vec{u}_i(t)$ is the unit vector of the molecular axis, and $\theta(t)$ is the angle between $\vec{u}_i(t)$ and $\vec{u}_i(0)$. When the rotational correlation function decays non-exponentially with time, it is often described by the Kohlrausch expression:

$$C_\ell(t) \propto \exp[-(t/\tau_\ell)^{\beta_\ell}], \quad \beta_\ell \leq 1. \tag{4}$$

In the present case, it was well reproduced with the fractional exponent, $\beta_\ell = 0.5-1.0$.

XRD experiments. Powder XRD measurements of dry and wet SWCNT samples were performed using synchrotron radiation X-rays with a wavelength of $\lambda = 0.100$ nm at the BL8B station of the Photon Factory, High Energy Accelerator Research Organization (KEK), Japan. The diffracted X-rays were recorded with an imaging plate. The resolution for the scattering angle 2θ, of the diffracted X-rays was 0.03°. For a wet sample, the SWCNT films were sealed inside a XRD quartz capillary with saturated water (H_2O) vapor of ultrahigh purity at RT. The dry sample was sealed after it was evacuated. The amplitude of the X-ray scattering wave vector is defined by $Q = 4\pi \sin \theta/\lambda$. The sample temperature was controlled by a gas-blow type cryostat (Rigaku) in the temperature range of 100–350 K. XRD studies for 1.4–2.40 nm SWCNT-water samples have been reported previously[22,28]. The results for the 4 nm SWCNT sample is shown in Supplementary Fig. S4.

Data availability. All data generated or analysed during this study are included in this published article and its Supplementary Information files.

References
1. Noy, A., Grigoropoulos, C. P. & Bakajin, O. Nanofluidics in carbon nanotubes. *Nano Today* **2**, 22–29 (2007).
2. Howorka, S. & Siwy, Z. Nanopore analytics: sensing of single molecules. *Chem. Soc. Rev.* **38**, 2360–2384 (2009).

3. Bocquet, L. & Charlaix, E. Nanofluidics, from bulk to interfaces. *Chem. Soc. Rev.* **39**, 1073–1095 (2010).
4. Rasaiah, J. C., Garde, S. & Hummer, G. Water in nonpolar confinement: from nanotubes to proteins and beyond. *Annu. Rev. Phys. Chem.* **59**, 713–740 (2008).
5. Aryal, P., Sansom, M. S. & Tucker, S. J. Hydrophobic gating in ion channels. *J. Mol. Bio.* **427**, 121–130 (2015).
6. Bellissent-Funel, M. C. *et al.* Water determines the structure and dynamics of proteins. *Chem. Rev.* **116**, 7673–7697 (2016).
7. Mishima, O. & Stanley, H. E. The relationship between liquid, supercooled and glassy water. *Nature* **396**, 329–335 (1998).
8. Debenedetti, P. G. Supercooled and glassy water. *J. Phys.: Condens. Matter* **15**, R1669–R1726 (2003).
9. Stanley, H. E. *et al.* The puzzling unsolved mysteries of liquid water: Some recent progress. *Physica A* **386**, 729–743 (2007).
10. Bertrand, C. E., Zhang, Y. & Chen, S. H. Deeply-cooled water under strong confinement: neutron scattering investigations and the liquid–liquid critical point hypothesis. *Phys. Chem. Chem. Phys.* **15**, 721–745 (2013).
11. Yoshida, K., Yamaguchi, T., Kittaka, S., Bellissent-Funel, M. C. & Fouquet, P. Neutron spin echo measurements of monolayer and capillary condensed water in MCM-41 at low temperatures. *J. Phys.: Condens. Matter* **24**, 064101 (2012).
12. Chu, X. Q., Liu, K. H., Tyagi, M. S., Mou, C. Y. & Chen, S. H. Low-temperature dynamics of water confined in a hydrophobic mesoporous material. *Phys. Rev. E* **82**, 020501 (2010).
13. Nagoe, A., Iwaki, S., Oguni, M. & Tôzaki, K. I. Pressure Dependence of the Liquid–Liquid Phase Transition of Nanopore Water Doped Slightly with Hydroxylamine, and a Phase Behavior Predicted for Pure Water. *J. Phys. Soc. Jpn.* **83**, 094601 (2014).
14. Demontis, P., Gulín-González, J., Masia, M. & Suffritti, G. B. The behaviour of water confined in zeolites: molecular dynamics simulations versus experiment. *J. Phys.: Condens. Matter* **22**, 284106 (2010).
15. Mazza, M. G., Stokely, K., Pagnotta, S. E., Bruni, F., Stanley, H. E. & Franzese, G. More than one dynamic crossover in protein hydration water. *Proc. Natl. Acad. Sci. USA* **108**, 19873–19878 (2011).
16. Cerveny, S., Mallamace, F., Swenson, J., Vogel, M. & Xu, L. Confined water as model of supercooled water. *Chem. Rev.* **116**, 7608–7625 (2016).
17. Swenson, J. & Teixeira, J. The glass transition and relaxation behavior of bulk water and a possible relation to confined water. *J. Chem. Phys.* **132**, 014508 (2010).
18. Bruni, F., Mancinelli, R. & Ricci, M. A. Multiple relaxation processes versus the fragile-to-strong transition in confined water. *Phys. Chem. Chem. Phys.* **13**, 19773–19779 (2011).
19. Brovchenko, I. & Oleinikova, A. Effect of confinement on the liquid-liquid phase transition of supercooled water. *J. Chem. Phys.* **126**, 214701 (2007).
20. Kumar, P., Han, S. & Stanley, H. E. Anomalies of water and hydrogen bond dynamics in hydrophobic nanoconfinement. *J. Phys.: Condens. Matter* **21**, 504108 (2009).
21. Xu, L. & Molinero, V. Is There a Liquid–Liquid Transition in Confined Water? *J. Phys. Chem. B* **115**, 14210–14216 (2011).
22. Kyakuno, H. *et al.* Diameter-dependent hydrophobicity in carbon nanotubes. *J. Chem. Phys.* **145**, 064514 (2016).
23. Koga, K., Gao, G. T., Tanaka, H. & Zeng, X. C. Formation of ordered ice nanotubes inside carbon nanotubes. *Nature* **412**, 802–805 (2001).
24. Maniwa, Y. *et al.* Phase transition in confined water inside carbon nanotubes. *J. Phys. Soc. Jpn.* **71**, 2863–2866 (2002).
25. Maniwa, Y. *et al.* Ordered water inside carbon nanotubes: formation of pentagonal to octagonal ice-nanotubes. *Chem. Phys. Lett.* **401**, 534–538 (2005).
26. Bai, J., Wang, J. & Zeng, X. C. Multiwalled ice helixes and ice nanotubes. *Proc. Natl. Acad. Sci. USA* **103**, 19664–19667 (2006).
27. Takaiwa, D., Hatano, I., Koga, K. & Tanaka, H. Phase diagram of water in carbon nanotubes. *Proc. Natl. Acad. Sci. USA* **105**, 39–43 (2008).
28. Kyakuno, H. *et al.* Confined water inside single-walled carbon nanotubes: Global phase diagram and effect of finite length. *J. Chem. Phys.* **134**, 244501 (2011).
29. Abragam, A. *Principles of Nuclear Magnetism* (Oxford, London 1961).
30. Farrar, T. C. & Becker, E. D. *Pulse and Fourier Transform NMR* (Academic Press. Inc., London 1971).
31. Ghosh, S., Ramanathan, K. V. & Sood, A. K. Water at nanoscale confined in single-walled carbon nanotubes studied by NMR. *Europhys. Lett.* **65**, 678–684 (2004).
32. Matsuda, K., Hibi, T., Kadowaki, H., Kataura, H. & Maniwa, Y. Water dynamics inside single-wall carbon nanotubes: NMR observations. *Phys. Rev. B* **74**, 073415 (2006).
33. Maniwa, Y. *et al.* Water-filled single-wall carbon nanotubes as molecular nanovalves. *Nat. Mater.* **6**, 135–141 (2007).
34. Chen, Q. *et al.* Identification of Endohedral Water in Single-Walled Carbon Nanotubes by ¹H NMR. *Nano Lett.* **8**, 1902–1905 (2008).
35. Mao, S., Kleinhammes, A. & Wu, Y. NMR study of water adsorption in single-walled carbon nanotubes. *Chem. Phys. Lett.* **421**, 513–517 (2006).
36. Das, A. *et al.* Single-File Diffusion of Confined Water Inside SWNTs: An NMR Study. *ACS Nano* **4**, 1687–1695 (2010).
37. Liu, X., Pan, X., Zhang, S., Han, X. & Bao, X. Diffusion of water inside carbon nanotubes studied by pulsed field gradient NMR spectroscopy. *Langmuir* **30**, 8036–8045 (2014).
38. Hata, K., Futaba, D. N., Mizuno, K., Namai, T. & Yumura, M. Iijima, S. Water-assisted highly efficient synthesis of impurity-free single-walled carbon nanotubes. *Science* **306**, 1362–1364 (2004).
39. Saito, T., Xu, W. C., Ohshima, S., Ago, H., Yumura, M. & Iijima, S. Supramolecular Catalysts for the Gas-phase Synthesis of Single-walled Carbon Nanotubes. *J. Phys. Chem. B* **110**, 5849–5853 (2006).
40. Saito, T., Ohshima, S., Okazaki, T., Ohmori, S., Yumura, M. & Iijima, S. Selective diameter control of single-walled carbon nanotubes in the gas-phase synthesis. *J. Nanosci. Nanotechnol.* **8**, 6153–6157 (2008).
41. Nakai, Y. *et al.* Observation of the intrinsic magnetic susceptibility of highly purified single-wall carbon nanotubes. *Phys. Rev. B* **92**, 041402 (2015).
42. Bloembergen, N., Purcell, E. M. & Pound, R. V. Relaxation Effects in Nuclear Magnetic Resonance Absorption. *Phys. Rev.* **73**, 679–746 (1948).
43. Ropp, J., Lawrence, C., Farrar, T. C. & Skinner, J. L. Rotational motion in liquid water is anisotropic: a nuclear magnetic resonance and molecular dynamics simulation study. *J. Am. Chem. Soc.* **123**, 8047–8052 (2001).
44. Wang, H. J., Xi, X. K., Kleinhammes, A. & Wu, Y. Temperature-Induced Hydrophobic-Hydrophilic Transition Observed by Water Adsorption. *Science* **322**, 80–83 (2008).
45. Kyakuno, H. *et al.* Amorphous water in three-dimensional confinement of zeolite-templated carbon. *Chem. Phys. Lett.* **571**, 54–60 (2013).
46. Soper, A. K. & Ricci, M. A. Structures of high-density and low-density water. *Phys. Rev. Lett.* **84**, 2881–2884 (2000).
47. Berendsen, H. J. C., Grigera, J. R. & Straatsma, T. P. The missing term in effective pair potentials. *J. Phys. Chem.* **91**, 6269–6271 (1987).
48. Chu, X. Q., Kolesnikov, A. I., Moravsky, A. P., Garcia-Sakai, V. & Chen, S. H. Observation of a dynamic crossover in water confined in double-wall carbon nanotubes. *Phys. Rev. E* **76**, 021505 (2007).
49. Rosenstihl, M., Kämpf, K., Klameth, F., Sattig, M. & Vogel, M. Dynamics of interfacial water. *J. Non-Cryst. Solids* **407**, 449–458 (2015).
50. Liu, L. *et al.* Quasielastic and inelastic neutron scattering investigation of fragile-to-strong crossover in deeply supercooled water confined in nanoporous silica matrices. *J. Phys.: Condens. Matter* **18**, S2261 (2006).

51. Faraone, A., Liu, K. H., Mou, C. Y., Zhang, Y. & Chen, S. H. Single particle dynamics of water confined in a hydrophobically modified MCM-41-S nanoporous matrix. *J. Chem. Phys.* **130**, 134512 (2009).
52. Harrach, M. F., Klameth, F., Drossel, B. & Vogel, M. Effect of the hydroaffinity and topology of pore walls on the structure and dynamics of confined water. *J. Chem. Phys.* **142**, 034703 (2015).
53. Laage, D. & Thompson, W. H. Reorientation dynamics of nanoconfined water: Power-law decay, hydrogen-bond jumps, and test of a two-state model. *J. Chem. Phys.* **136**, 044513 (2012).
54. Morishige, K. & Uematsu, H. The proper structure of cubic ice confined in mesopores. *J. Chem. Phys.* **122**, 044711 (2005).
55. Nagoe, A., Kanke, Y., Oguni, M. & Namba, S. Findings of C_p Maximum at 233 K for the Water within Silica Nanopores and Very Weak Dependence of the T_{max} on the Pore Size. *J. Phys. Chem. B* **114**, 13940–13943 (2010).
56. Morishige, K. & Kawano, K. Freezing and melting of water in a single cylindrical pore: The pore-size dependence of freezing and melting behavior. *J. Chem. Phys.* **110**, 4867–4872 (1999).
57. Hinze, G. & Diezemann, G. & Basché, Th. Rotational Correlation Functions of Single Molecules. *Phys. Rev. Lett.* **93**, 203001 (2004).

Acknowledgements

Author Contributions

H.K. performed all experiments and data analyses. K.M., Y.N. and Y. Miyata provided advice during the experiments and data analysis. K.M. also assisted during the NMR experiments. R.I. assisted during the NMR, DSC and XRD measurements. T.S. and K.H. prepared the SWCNT samples, and Y. Maniwa organized the study. The manuscript was completed by all the authors.

Additional Information

Supplementary information accompanies this paper at https://doi.org/10.1038/s41598-017-13704-6.

Competing Interests: The authors declare that they have no competing interests.

Publisher's note: Springer Nature remains neutral with regard to jurisdictional claims in published maps and institutional affiliations.